ELSEVIER

Microelectronics Journal 33 (2002) 141–151

Microelectronics Journal

www.elsevier.com/locate/mejo

Differential oversampling data converters in SEED technology

S.F. Al-Sarawi[a,*], P.B. Atanackovic[b], W. Marwood[b], B.A. Clare[c], K.A. Corbett[b], K.J. Grant[b], J. Munch[c]

[a]*Department of Electrical and Electronic Engineering, The Centre for High Performance Integrated Technologies and Systems (CHiPTec), Adelaide University, Adelaide, SA 5005, Australia*

[b]*Communications Division, Defence Science and Technology Organisation, P.O. Box 1500, Salisbury, SA 5108, Australia*

[c]*Department of Physics and Mathematical Physics, Adelaide University, Adelaide, SA 5005, Australia*

Accepted 21 August 2001

Abstract

Differential architectures for both first order error diffusion and first order sigma–delta modulators are presented in this paper. Techniques required to transform single-ended architectures to differential architectures are discussed which are suitable for implementation in both p–i–n and n–i–n SEED technologies. Descriptions of common SEED circuit modules, together with SPICE behavioural simulations are also presented. A feature of the architectures presented is that they can be fully integrated into a single substrate using MEMS technology. This can be done by incorporating integrated optical waveguides together with MMIC technology. The goal of this work is a fully integrated differential optical oversampling modulator with extremely high resolution and linearity. © 2002 Published by Elsevier Science Ltd.

Keywords: Optoelectronic data converter; Very high speed data converter; Oversampling data converter; Photonic data converter; Sigma–delta modulators

1. Introduction

Data converters play an important role in most digital signal processing systems as they provide an interface between the inherently analog world and the digital representation used in data processing applications. The requirement for these converters varies depending on the specific application. For example, wideband communications surveillance systems and digital radio receivers require high speed, high resolution and high linearity whereas generic wideband electronic systems require very high speed converters but with less demanding specifications for resolution and linearity [12]. Although conventional Nyquist rate data converters can fulfill the high speed requirements of wideband surveillance systems, the very demanding resolution and linearity requirements are the limiting factors. Oversampling data converters can provide the required resolution and linearity, but not at the required speed. The common technologies currently used for designing oversampling data converters are CMOS and GaAs. The maximum speed of the converters is limited both by the maximum switching speed of the devices and also by the unavoidable interconnect parasitics such as resistance, inductance and capacitance. To alleviate the limitation of current CMOS and GaAs technologies researchers are studying the use of photonic technologies in designing data converters. Examples in the literature where photonics have been used to overcome the limitations of electrical interconnect and switching speeds are described in Refs. [4–7]. By combining the switching speed of optoelectronic devices with micro electro mechanical systems (MEMS) technology it is possible to build very high speed, high density optoelectronic circuits which can be integrated into very high data rate, lightweight, low cost fully integrated optoelectronic systems. An improved self electro-optic effect device (SEED) called the n–i(MQW)–n SEED has been developed [3]. This device has great potential for high speed data converter applications as it offers a low operating power, and a symmetric *I–V* curve which is contrasted with the unipolar *I–V* curve of the single ended p–i–n device. This paper presents and discusses oversampling modulator architectures that are suited for both p–i–n and n–i–n technologies. These modulators rely on high oversampling ratios to obtain high resolution and linearity. One of their main advantages is a very high tolerance for circuit imperfections, especially when two level quantisation is employed. This attribute is highly desirable when using devices at very high operating speeds and with relatively poorly controlled circuit parameters. In

* Corresponding author. Tel.: +61-8-8303-4705; fax: +61-8-8303-4360.
E-mail address: alsarawi@eleceng.adelaide.edu.au (S.F. Al-Sarawi).

0026-2692/02/$ - see front matter © 2002 Published by Elsevier Science Ltd.
PII: S0026-2692(01)00113-6

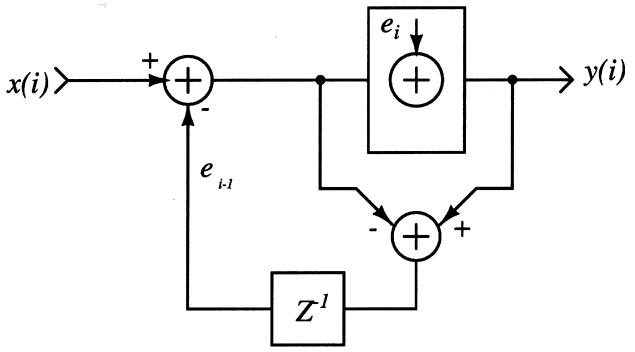

Fig. 1. A first order error diffusion modulator.

the literature a number of papers discuss the implementation of optical oversampling data converters [16,17,19] which take advantage of high speed, low jitter optical clocks.

In contrast to prior work this paper presents a fully differential SEED approach for implementation of a fully integrated oversampling data converter that can use either an optical or electrical signal as an input. In the following discussion, an oversampling modulator architecture is presented in two forms that are mathematically equivalent. These forms are the first order error diffusion modulator and the first order sigma–delta modulator. These two representations were chosen as they present the basic components that are needed in designing high order oversampling modulators. In contrast to electric signals, optical beams are unipolar. Hence, common modulator architectures cannot be applied directly to optical modulator designs. The work published by Willis et al. [19] on unipolar loop signals in the error diffusion modulator represents a possible approach for implementation with SEED technology. The modification required for the optical error diffusion architecture is an adjustment of the quantiser threshold and a constraint on the input signal amplitude in order to obtain a unipolar signal at all intermediate nodes in the modulator. However, a better approach is to encode the input signal as the difference between two unipolar signals and perform all modulator operations using differential optical signals. With this approach, no restriction on the input signal amplitude or adjustment of the quantiser threshold is needed. Sections 2 and 3 present and discuss the formulae for a differential first order error diffusion modulator and a differential first order sigma–delta modulator, respectively. Section 4 presents the self electro-optic effect devices (SEEDs) and their characteristics and briefly discusses some of the basic modules that are needed for the design and implementation of the differential modulator. Sections 5 and 6 present possible implementations. Note that in this paper the filtering and decimation circuitry needed to reduce the output bit rate of the modulator is not discussed.

2. Differential error diffusion modulator

One of the simplest forms of oversampling modulator is the error diffusion modulator shown in Fig. 1. The modulator consists of (i) an analog add–subtract circuit, (ii) a quantiser and (iii) a unit delay element. The output signal, $y(i)$, for the error diffusion modulator can be written as

$$y(i) = x(i) + e_i(1 - Z^{-1}). \tag{1}$$

For the purpose of simplicity the differential error diffusion architecture is presented before the theoretical analysis of the modulator and is shown in Fig. 2. It is assumed that the input signal to the modulator can be either optical or electrical. The architecture has a single-ended to differential converter, a differential analog adder circuit and a differential quantiser. The output from the single-to-differential block can be written as

$$P_{\mathrm{in_H}} = P_{\mathrm{os}} + P_{\mathrm{in}}(x(i))/2. \tag{2}$$

$$P_{\mathrm{in_L}} = P_{\mathrm{os}} - P_{\mathrm{in}}(x(i))/2. \tag{3}$$

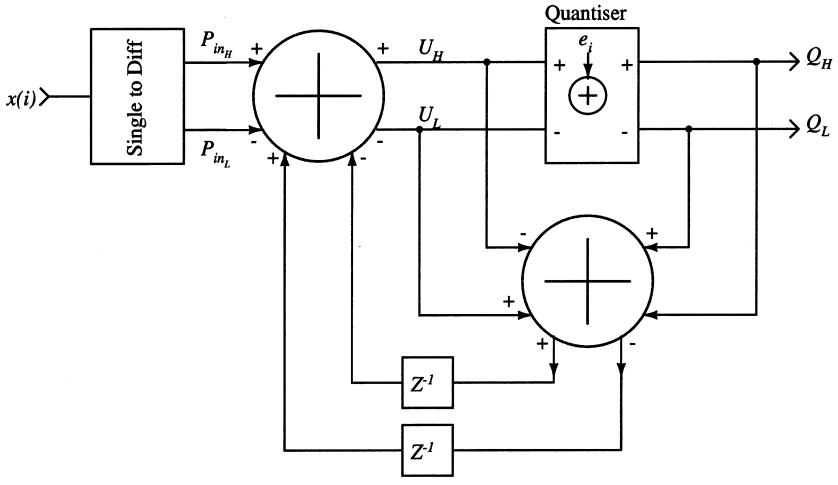

Fig. 2. A differential first order error diffusion modulator.

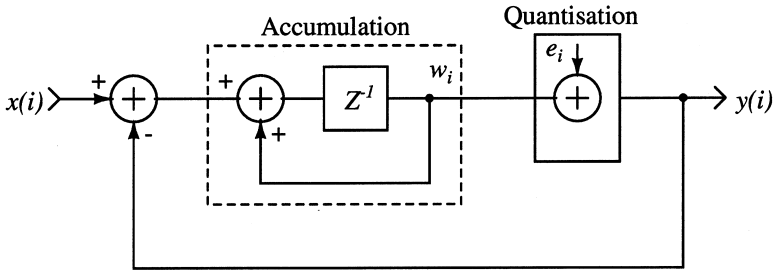

Fig. 3. A first order sigma–delta modulator.

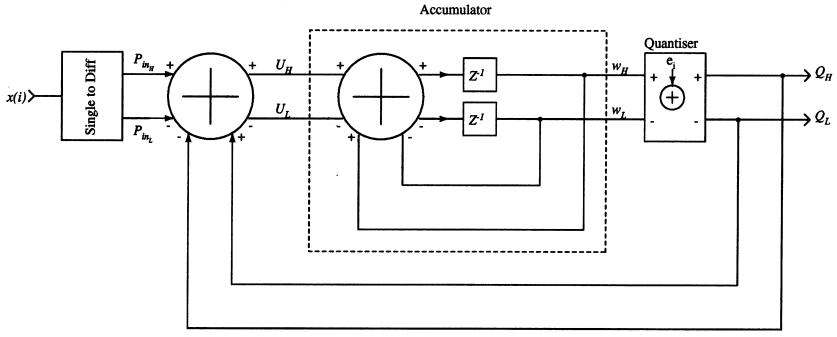

Fig. 4. A differential first order sigma–delta modulator.

The differential output of the analog adders $(U_H - U_L)$ can be written as

$$(U_H - U_L) = \frac{Z^{-1}}{(1 - Z^{-1})}(Q_L - Q_H) + \frac{P_{in}(x(i))}{(1 - Z^{-1})}; \qquad (4)$$

while the quantiser differential output $(Q_H - Q_L)$ can be written as

$$(Q_H - Q_L) = (U_H - U_L) + e_i. \qquad (5)$$

Substituting the adder's differential output from Eq. (4)

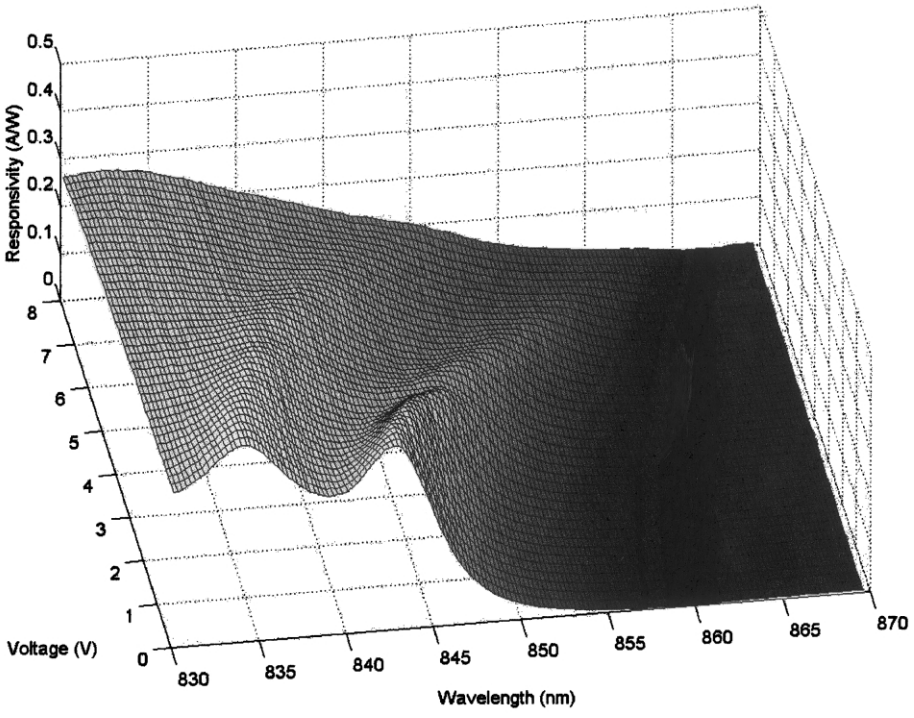

Fig. 5. Experimental measurement of the responsivity of a p–i(MQW)–n diode.

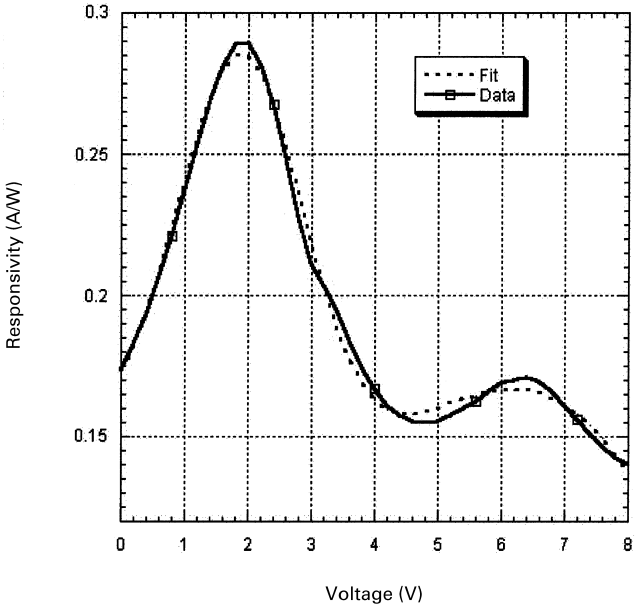

Fig. 6. Comparison of semi-empirical fit and experimental data for a p–i(MQW)–n SEED diode.

into Eq. (5) results in

$$(Q_{\mathrm{H}} - Q_{\mathrm{L}}) = P_{\mathrm{in}}(x(i)) + e_i(1 - Z^{-1}). \tag{6}$$

Comparing Eq. (6) with Eq. (1) shows that both the results are equivalent and that the output from the quantiser is differential. Furthermore, simulating the differential modulator shows identical behaviour to the first order error diffusion modulator.

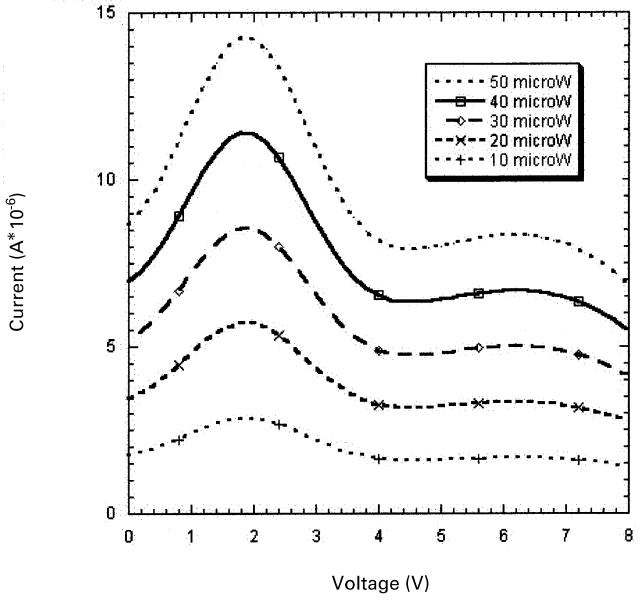

Fig. 7. Simulated SEED current vs. bias, showing the effect of increasing optical power.

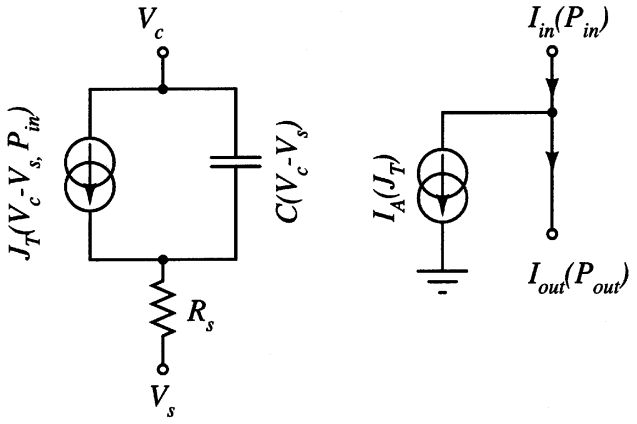

Fig. 8. SEED equivalent circuit.

3. Differential sigma–delta modulator

A block diagram of a first order sigma–delta modulator is shown in Fig. 3. The output signal of this modulator can be written as

$$y(i) = x(i)Z^{-1} + e(i)(1 - Z^{-1}). \tag{7}$$

The same methodology used in the design of a differential error diffusion modulator can be applied to the design of a differential sigma–delta modulator. The new differential sigma–delta modulator is shown in Fig. 4. The analysis of this modulator can be carried out as follows. Using Eqs. 2 and 3, $(U_{\mathrm{H}} - U_{\mathrm{L}})$ and $(W_{\mathrm{H}} - W_{\mathrm{L}})$ can be written as

$$(U_{\mathrm{H}} - U_{\mathrm{L}}) = (P_{\mathrm{in_H}} - P_{\mathrm{in_L}}) - (Q_{\mathrm{H}} - Q_{\mathrm{L}}). \tag{8}$$

$$(W_{\mathrm{H}} - W_{\mathrm{L}}) = (U_{\mathrm{H}} - U_{\mathrm{L}})\frac{Z^{-1}}{1 - Z^{-1}}. \tag{9}$$

Also, the quantiser output $(Q_{\mathrm{H}} - Q_{\mathrm{L}})$ can be written as

$$(Q_{\mathrm{H}} - Q_{\mathrm{L}}) = (W_{\mathrm{H}} - W_{\mathrm{L}}) + e(i). \tag{10}$$

Substituting Eq. (8) in Eq. (9) and then substituting the results into Eq. (10) gives

$$(Q_{\mathrm{H}} - Q_{\mathrm{L}}) = P_{\mathrm{in}}(x(i))Z^{-1} + e_i(1 - Z^{-1}). \tag{11}$$

When the above equations of the differential sigma–delta modulator were implemented in Matlab the results, as expected, were identical to those of the first order sigma–delta modulator.

4. SEED circuit modules

This section presents a SPICE model for the SEED and SPICE simulation results for some of the basic SEED circuit modules that are needed to implement the differential modulators discussed earlier. Detailed discussion of the p–i(MQW)–n SEED and n–i(MQW)–n SEED devices can be found in Refs. [2,13], while detailed discussion of the operation of some of the presented circuits can be found

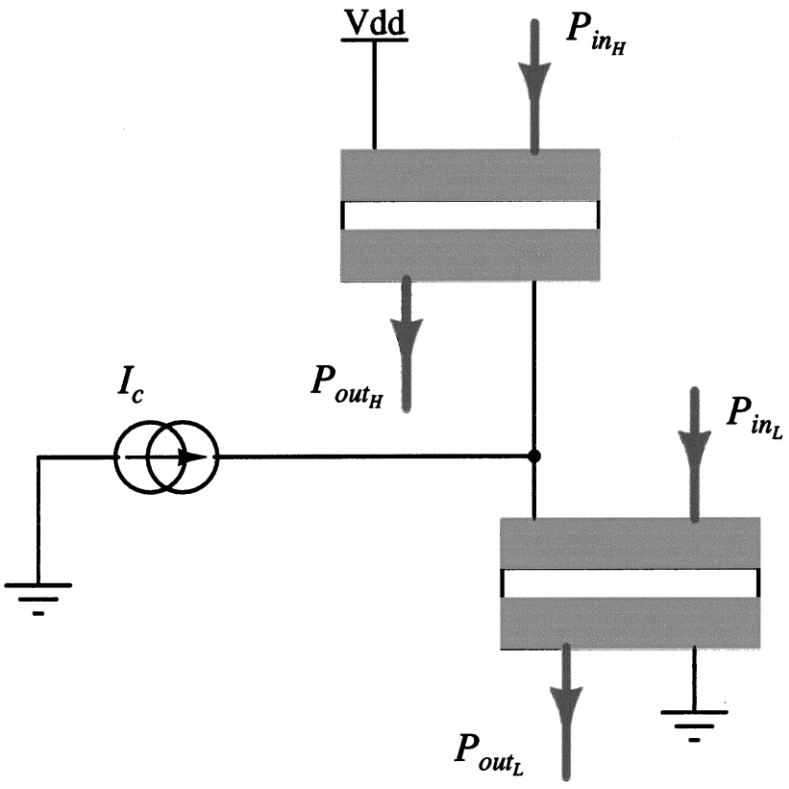

Fig. 9. A differential self-linearised modulator circuit.

in Refs. [1,14]. In the following circuit, it is assumed that p–i–n or n–i–n devices are operating in the self-linearised mode unless otherwise mentioned. Detailed discussion of this mode of operation is given in Ref. [15]. In the following diagrams, thick paths indicate an optical connection and thin paths represent an electrical connection.

4.1. p–i–n SEED model

SEEDs are fabricated using molecular beam epitaxy (MBE) techniques to grow a series of narrow band gap (GaAs) and wide band gap (AlGaAs) layers with nanometer resolution. The result of these growths is a series of quantum potential wells in the conduction and valence bands, and is referred to as a multiple quantum well (MQW) structure. Applying an electric field perpendicular to the plane of the MQW layers reduces the photon energy required to create an electron–hole pair, resulting in a redshift in the absorption spectrum of the structure. This effect is commonly referred to as the quantum confined stark effect (QCSE) [8].

To illustrate the QCSE, the responsivity of a p–i(MQW)–n SEED was measured as the applied bias and wavelength were varied. The results in Fig. 5 clearly show that the large and small peak, known as the heavy and light hole excitons respectively, move to longer wavelength and decrease in amplitude as the applied bias is increased.

A semi-empirical model of QCSE for circuit simulation can be described as follows. The current density, at a given

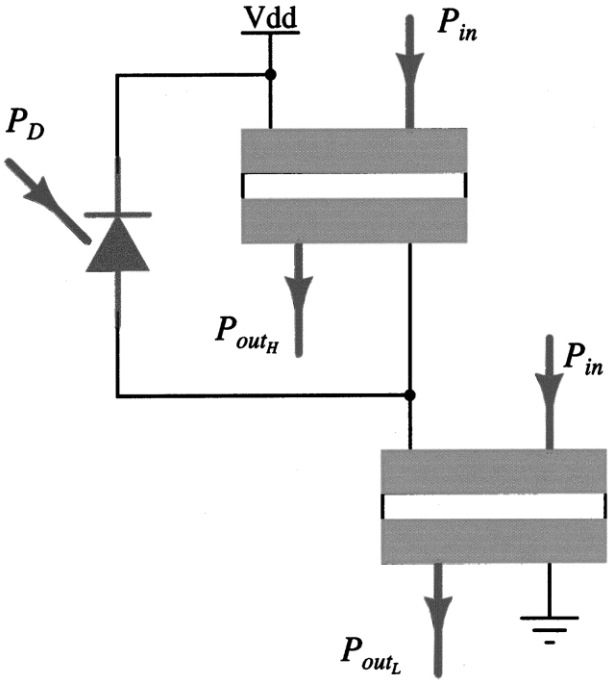

Fig. 10. A single ended optical input to differential optical output circuit.

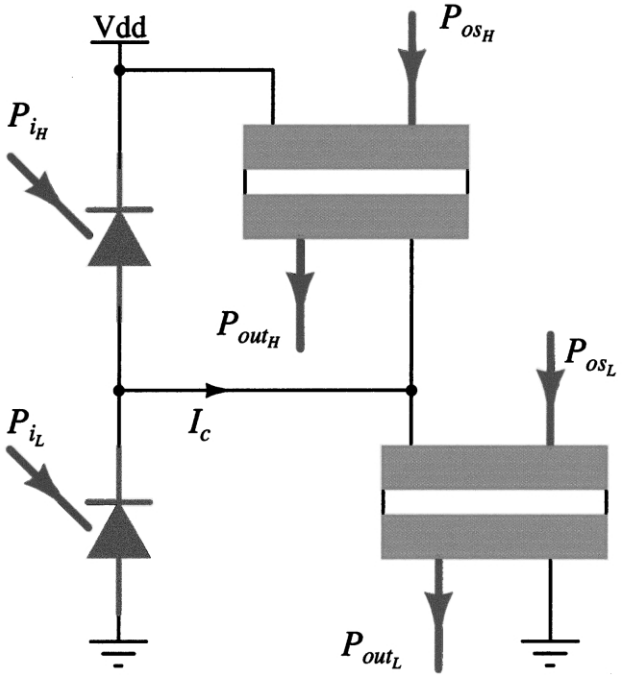

Fig. 11. A differential optical input differential optical output circuit.

wavelength, due to the MQW absorption can be modelled as

$$J_T(V, P_{in}) = P_{in}(\beta_{hh} \exp(-0.5((V - \sigma_{hh})/\Gamma_{hh})^2) + \beta_{lh} \exp(-0.5((V - \sigma_{lh})/\Gamma_{lh})^2) + \alpha_1 V + \alpha_2), \quad (12)$$

where P_{in} is the input power and Γ_i, β_i and σ_i are the width, strength and position of the excitonic responses. The subscripts hh and lh refer to the heavy hole and light hole excitons, V is the bias voltage across the device and α_1, α_2 are fitting parameters to model the continuum absorption. The model and experimental data for a wavelength of 846 nm are compared in Fig. 6.

The p–i(MQW)–n SEED equivalent circuit can be represented by (i) a non-linear voltage–current controlled current source described by J_T; (ii) a parallel voltage dependent capacitance $C(V)$ to represent the spatial separation of photocreated electron–hole pairs within the intrinsic MQW region; and (iii) a series resistance R_s due to the degenerately doped layers/ohmic contacts. The equivalent circuit for the p–i–n SEED is shown in Fig. 8. In the figure, J_T represents the current given in Eq. (12) and I_c is a current proportional to the voltage across the SEED device. The optical input and output powers are represented as current sources and labelled as $I_{in}(P_{in})$ and $I_{out}(P_{out})$ in the model. Fig. 7 shows the characteristics of the p–i–n SEED, using the model shown in Fig. 8 as a function of the voltage across the device at different input power levels.

4.2. Optical addition and subtraction

Fig. 9 presents a differential self-linearised modulator circuit [14]. The relation between the differential input power, $D_{in} = P_{in_H} - P_{in_L}$, and the differential output power, $D_{out} = P_{out_H} - P_{out_L}$, can be expressed as

$$D_{out} = D_{in} + \frac{\hbar\omega}{e} I_c. \quad (13)$$

where $\hbar\omega$ and e are the photon energy and the electron charge, respectively. By replacing the current source in

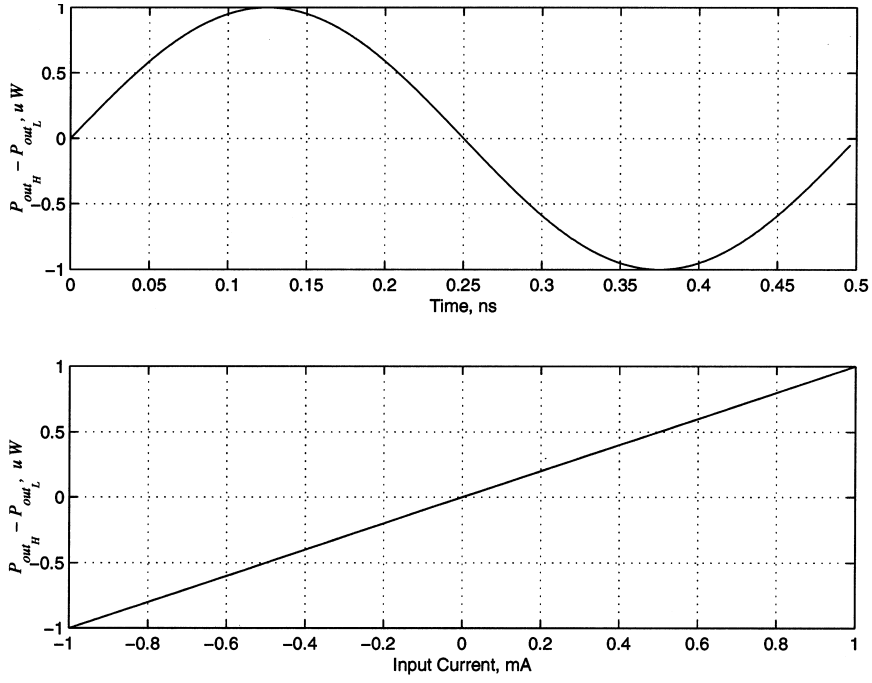

Fig. 12. Simulation results for the differential self-linearised modulator circuit shown in Fig. 9.

Fig. 9 with a photodiode with incident power P_D and setting $P_{in_H} = P_{in_L}$ as shown in Fig. 10 a single ended input optical power to a differential output optical power circuit can be obtained. The relation between the optical input power P_D and the output optical power can be written as

$$D_{out} = P_D. \tag{14}$$

An optical addition and subtraction circuit can also be designed based on the circuit shown in Fig. 9. This can be achieved by replacing the current source with two photodiodes as shown in Fig. 11. The relation between the input powers $D_i = P_{i_H} - P_{i_L}$, the optical bias power, $D_{os} = P_{os_H} - P_{os_L}$ and the output powers, $D_{out} = P_{out_H} - P_{out_L}$ can be written as

$$D_{out} = D_{os} + D_i. \tag{15}$$

The same circuit can be used for subtraction by simply interchanging either P_{i_H} and P_{i_L} or P_{os_H} and P_{os_L} in Fig. 11. The simulation results are consistent with the analysis and show the differential operation of the circuit. Using the p–i–n SEED circuit model discussed in Section 4.1, SPICE simulations were carried out and the results of the simulation for the differential SEED circuit are shown in Fig. 12. The input signal to the circuit shown in Fig. 11 can be either optical, electrical or both. For these simulations, a supply voltage of 6 V was used to ensure the SEED operated within the self-linearised region. Also, a strong optical bias signal, P_{os}, was used to maximise the input current dynamic range. For this simulation, a sinusoidal input current signal was used with a frequency of 2 GHz. It should be mentioned that these simulations represent idealised SEED operation.

4.3. Optical replication

Another important circuit to consider is the output replicating SEED shown in Fig. 13 [14]. In this figure, the input optical power source, P_{os}, is the same for all the SEEDs. Hence, their differential output is zero. The function of this circuit is to generate two identical outputs that are proportional to the input current or differential input power as mentioned earlier. The relation between the differential output power, $D_A = (P_{A_H} - P_{A_L})$ and $D_B = (P_{B_H} - P_{B_L})$, and the differential input powers, $D_{in} = (P_{in_H} - P_{in_L})$ can be written as

$$D_A = D_{in} \text{ and } D_B = D_{in}. \tag{16}$$

The simulation results for the replicating circuit are shown in Fig. 14. The simulation shows that two equal differential outputs are generated which are equal to the differential input power applied to the photodiodes.

4.4. Optical quantiser

A quantiser can be formed using two p–i–n or n–i–n devices as shown in Fig. 15. Such a configuration is commonly referred to as a symmetrical SEED or S-SEED. It should be mentioned that the SEEDs in this circuit are not operating in the self-linearised region of operation. The quantiser configuration has 'time-sequential gain', where the state of the S-SEED can be set with a low power beam and subsequently read out with a high power beam P_{clk}. Detailed operation of such configurations can be found in Refs. [9,11,18]. One problem with the S-SEED is the hysteresis in its I–V characteristics. A number of techniques to reduce this hysteresis have been presented in the literature Refs. [1,11]. The consequence of hysteresis in oversampling modulators is a reduction in the maximum SNR obtainable.

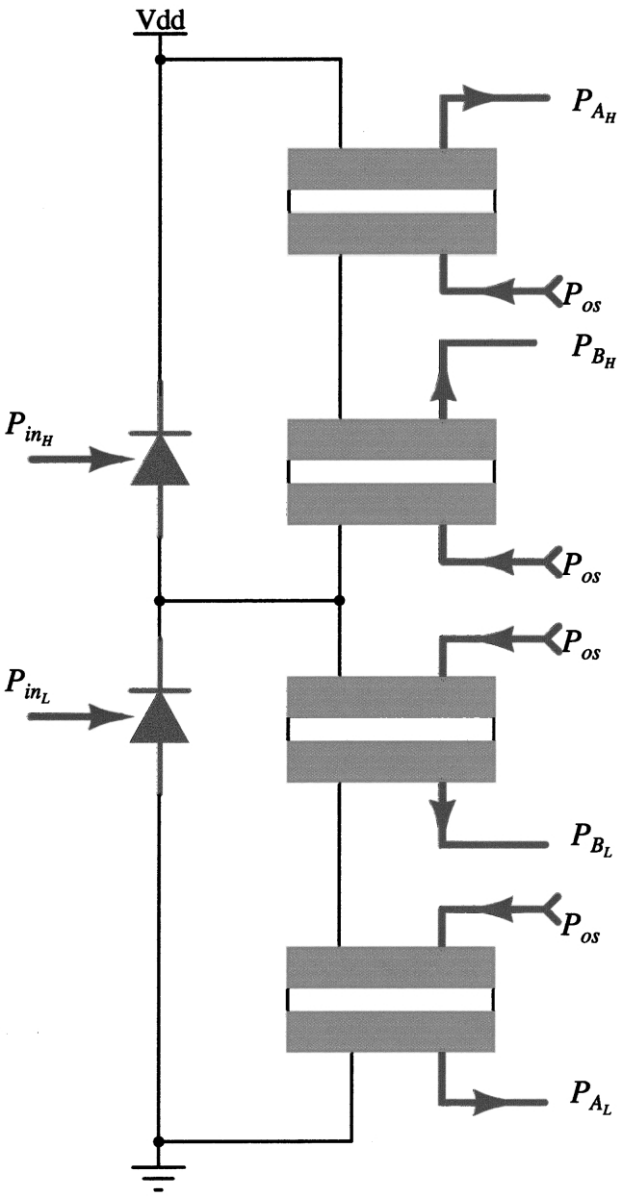

Fig. 13. An optical replicating circuit.

Using the developed device model the optical quantiser shown in Fig. 15 was simulated using HSPICE as shown in Fig. 16. The upper two simulations show the quantiser behaviour as a function of the differential optical power without the inclusion of an optical clock signal. The upper graph

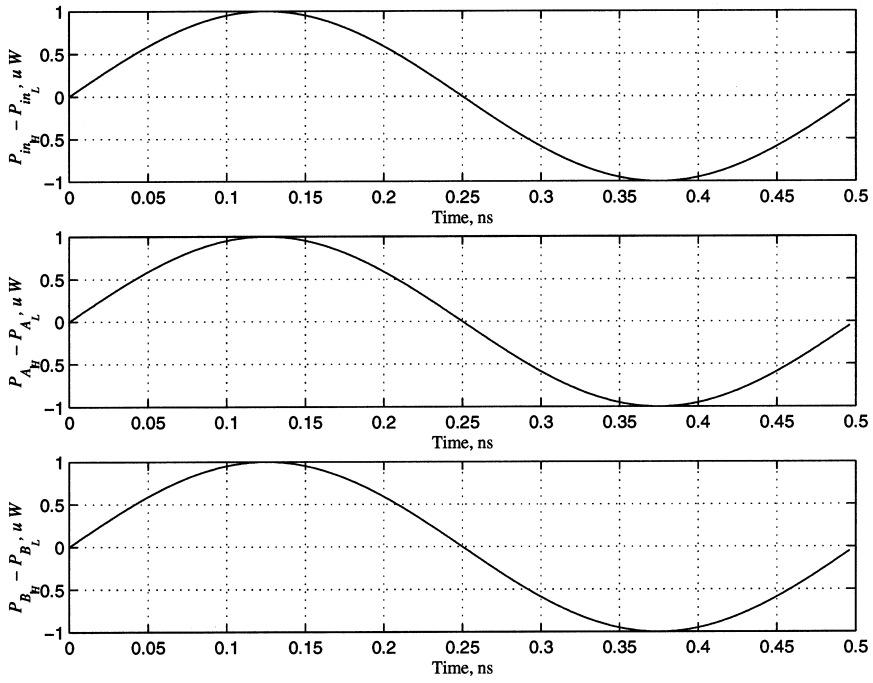

Fig. 14. Simulation of the optical replicating circuit shown in Fig. 13.

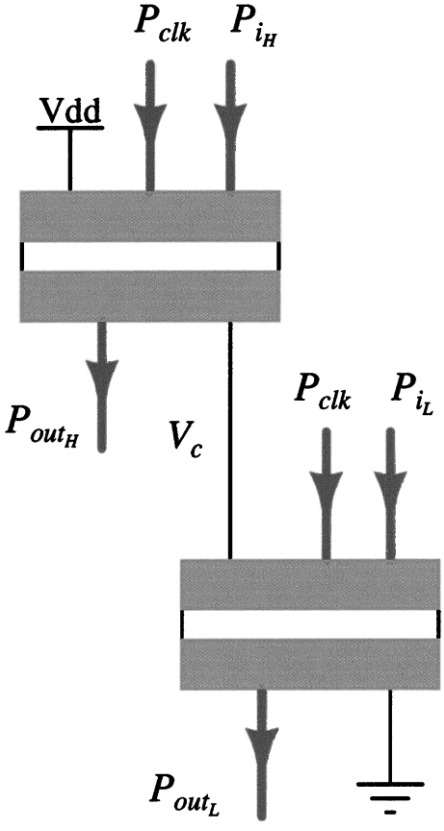

Fig. 15. A differential optical quantiser circuit.

shows the voltage at node V_c when two strong differential optical signals are applied, while the second from the top shows the voltage at V_c as a result of weaker differential optical signals. As expected the S-SEED structure exhibits hysteresis and the transition from one state to another is dependent on the optical signal strength. The last two simulations in Fig. 16 show the quantiser switching behaviour as a function of two weak optical signals. The last simulation shows the effect of applying the optical clock signal to both SEED devices to accelerate the device switching speed. All the presented simulations are consistent with optical quantiser behaviour described in the literature Refs. [10,18].

5. A fully differential SEED error diffusion modulator

The circuit modules discussed in Section 4 are combined in this section to design a fully differential error diffusion oversampling modulator based on the analysis presented in Section 2. The full modulator circuit is shown in Fig. 17. A direct comparison between this figure and the architecture shown in Fig. 2 shows that the single ended to differential circuit is merged with the differential add–subtract module. Furthermore, a replicating circuit is needed to provide a replica of the add–subtract result to both the quantiser and a second differential add–subtract module.

6. A fully differential SEED sigma–delta modulator

Adopting the same technique used in the differential

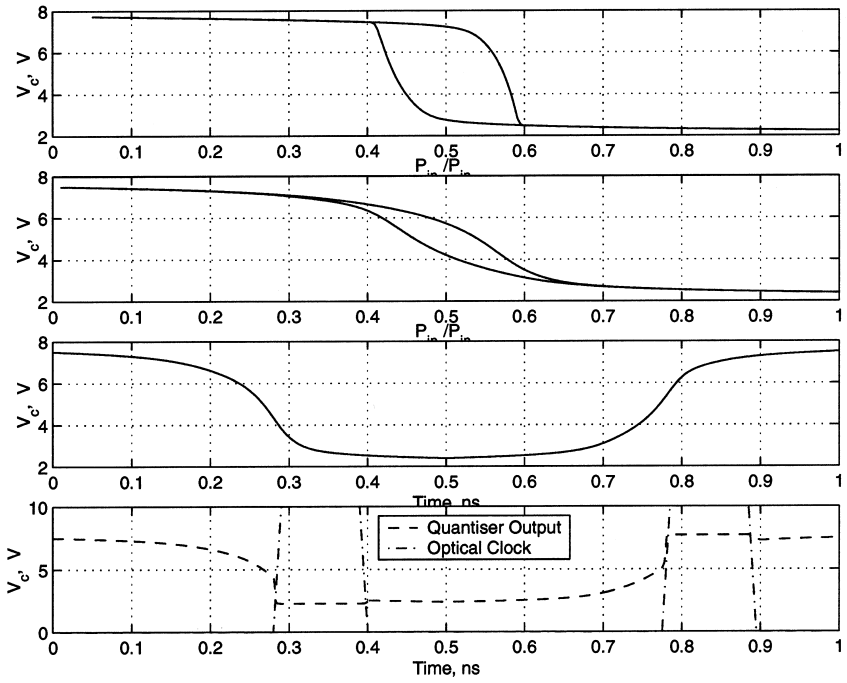

Fig. 16. Simulation of the quantiser SEED circuit shown in Fig. 15.

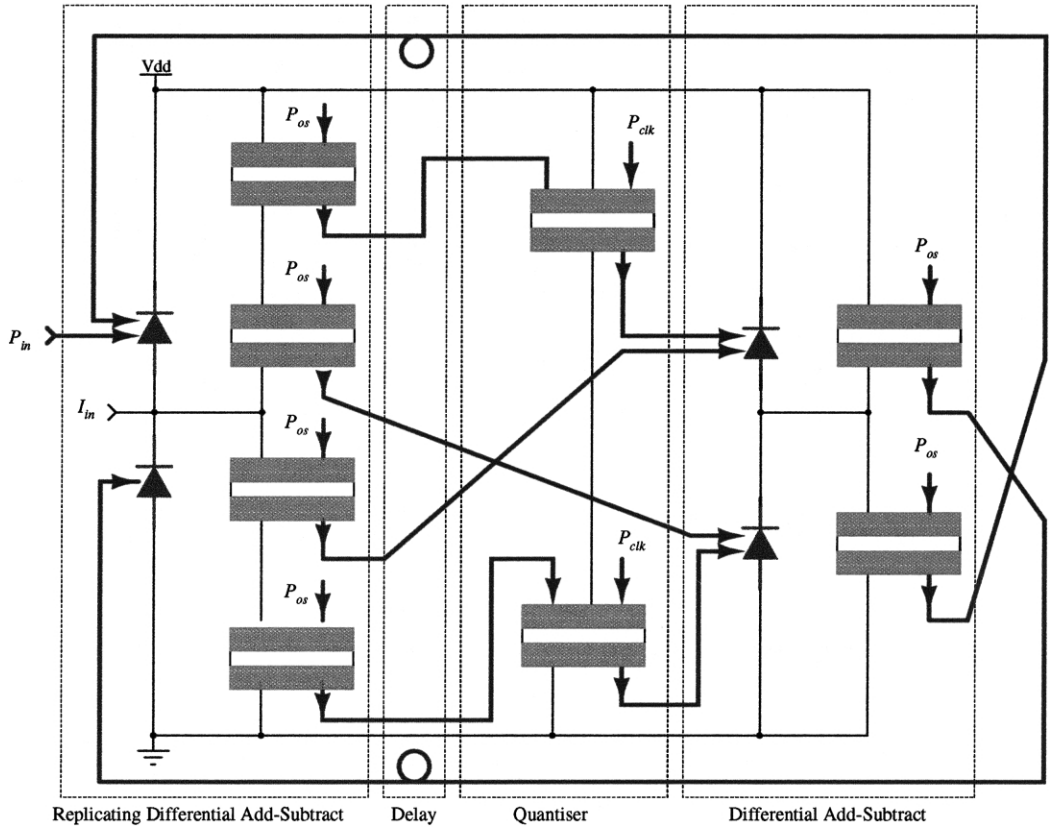

Fig. 17. A SEED implementation of the differential error diffusion architecture shown in Fig. 2.

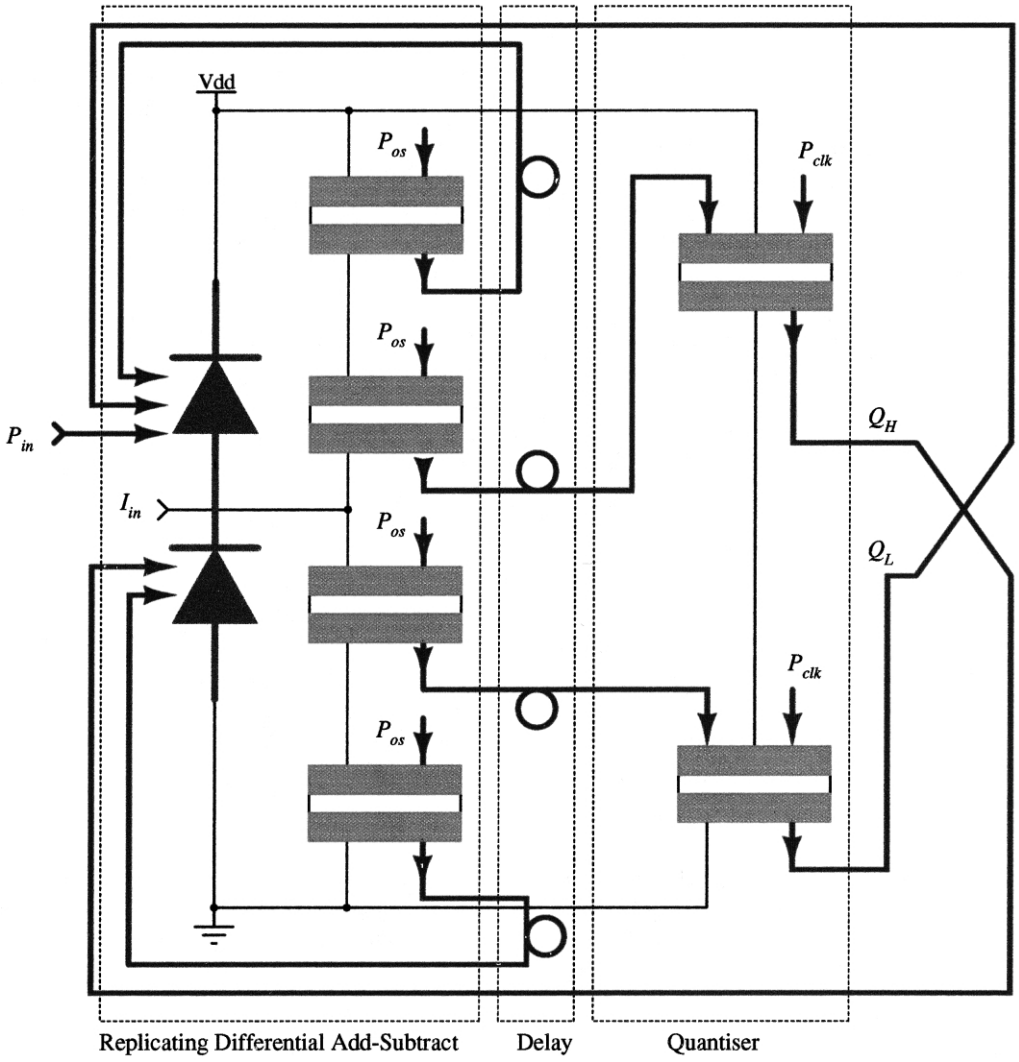

Fig. 18. A SEED implementation of the differential first order sigma–delta modulator architecture shown in Fig. 4.

SEED error diffusion modulator, it is possible to design a sigma–delta modulator. The new differential first order sigma–delta modulator is shown in Fig. 18. The implementation shown in this figure differs from the architecture shown in Fig. 4 in that only two delay elements are needed. However, in the implementation shown, four delay elements are used. The difference is due to a trade-off of one differential add–subtract SEED module for two extra delay elements. Comparing the interconnect complexity of the sigma–delta implementation to the differential error diffusion modulator shown in Fig. 2, it can be seen that the sigma–delta modulator has fewer optical waveguide intersections. This may simplify implementation.

7. Conclusion

Differential architectures for both first order error diffusion and first order sigma–delta modulators have been presented. These architectures are suitable for implementation in both p–i–n and n–i–n SEED technologies. A brief description of common SEED circuit modules, together with SPICE behavioural simulations, was also provided. These modules were then used in the design of differential optical first order error diffusion and sigma–delta modulators. The paper illustrates the techniques required to transform single-ended architectures to differential architectures. It is a straightforward process to extend the application of these techniques to higher order modulators. A feature of the architectures presented is that they can be fully integrated into a single substrate using MEMS technologies. This can be done by incorporating integrated optical waveguides together with MMIC technology. The goal of this work is a fully integrated differential optical oversampling modulator with extremely high resolution and linearity.

References

[1] S.F. Al-Sarawi, N. Burgess, W. Marwood, P.B. Atanackovic, Very high speed differential optoelectronic algorithmic ADC using n–i(MQW)–n Seed technology, in: B. Courtois, S. Demidenko (Eds.), Design, Characterization, and Packaging for MEMS and Microelectronics, 3893, SPIE, Queensland, Australia, 1999, pp. 284–295.

[2] P.B. Atanackovic, W. Marwood, A.P. Willis, G. Griffiths, An electro-optic logic family and ultra-high speed adder architecture: n–i(MQW)–n self electro-optic effect devices, Fourteenth Australian Microelectronics conference, IREE, Melbourne, Australia, October 1997, pp. 195–200

[3] Petar B. Atanackovic, Opto-electronic properties of II–VI strained-layer superlattices and heterostructures, PhD thesis, chapter 7, The University of Adelaide, December 1996.

[4] A.S. Bhushan, F. Coppinger, B. Jalali, Time-stretched analog-to-digital conversion, Electron. Lett. 34 (1998) 839–841.

[5] A.S. Bhushan, F. Coppinger, B. Jalali, Photonic sampling and time stretching for analog-to-digital conversion, Advanced A/D and D/A conversion techniques and their applications, IEE, July 1999, pp. 1–4.

[6] A.S. Bhushan, F. Coppinger, B. Jalali, S. Wang, H. Feterman, 150 Gsample/s wavelength division sampler with time stretched output, Electron. Lett. 13 (1998) 474–475.

[7] J. Cai, G.W. Taylor, An optoelectronic thyristor-based analog-to-digital converter for parallel processing, Appl. Phys. Lett. 73 (6) (1998) 2372–2374.

[8] H.S. Hinton, An Introduction to Photonic Switching Fabrics, Plenum Press, New York, 1993, pp. 175–176, Chapter 4.

[9] A.L. Lentine, H.S. Hinton, D.A.B. Miller, J.E. Henry, J.E. Cunningham, L.M.F. Chirovsky, Symmetric self-elecro-optic effect device: Optical set-reset latch, differential logic gate, and differential modulator/detector, IEEE J. Quant. Electron. 25 (8) (1989) 1928–1936.

[10] A.L. Lentine, D.A.B. Miller, J.E. Henry, J.E. Cunningham, M.F. Chirovsky, Multistate self-electro-optic effect devices, IEEE J. Quantum Electron. 25 (8) (1989) 1921–1927.

[11] L.M. Loh, J.L. LoCicero, Subnanosecond sampling all-optical analog-to-digital converter using symmetric self-electro-optic effect devices, Opt. Engng. 35 (2) (1996) 457–466.

[12] W. Marwood, P.B. Atanackovic, J. Munch, N. Burgess, S.F. Al-Sarawi, A MMIC compatible photonic A/D converter, Third International Conference on Advanced A/D and D/A Conversion Techniques and their Applications, IEE, Glasgow, UK, July 1999, pp. 17–20.

[13] D.A.B. Miller, Quantum well self-electro-optic effect devices, Opt. Quantum Electron. 22 (1990) S61–S98.

[14] D.A.B. Miller, Novel analog self-electrooptic-effect devices, IEEE J. Quantum Electron. 29 (1993) 678–698.

[15] D.A.B. Miller, D.S. Chemla, T.C. Damen, T.H. Wood, C.A. Burrus, A.C. Gossard, W. Wiegmann, The quantum well self-electrooptic effect device: optoelectronic bistability and oscillation, and self linearized modulation, IEEE J. Quantum Electron. 21 (1985) 1462–1476.

[16] P.E. Pace, S.J. Ying, R.J. Pieper, Integrated optical sigma–delta modulators, Opt. Engng 35 (7) (1996) 1828–1836.

[17] B.L. Shoop, Second-order cascaded optical error diffusion modulators for oversampled analog-to-digital converters, Opt. Commun. 102 (1 and 2) (1993) 125–132.

[18] A. Wachlowski, D. Rhein, J. Doppelbauer, W. Leeb, Device characteristics and modelling of symmetric self-electro-optic effect devices (S-SEED), Opt. Comput. Process. 2 (3) (1992) 189–197.

[19] A.P. Willis, D. Griffiths, P.B. Atanackovic, The use of unipolar loop signals in the error diffusion modulator, IEEE Trans. Circ. Syst. II 45 (12) (1998) 1597–1599.